Two-Phase Modeling of Mushy Zone Parameters Associated with Hot Tearing

IVAR FARUP and ASBJØRN MO

A two-phase continuum model for an isotropic mushy zone is presented. The model is based upon the general volume-averaged conservation equations, and quantities associated with hot tearing are included, *i.e.*, after-feeding of the liquid melt due to solidification shrinkage is taken into account as well as thermally induced deformation of the solid phase. The model is implemented numerically for a one-dimensional model problem with some similarities to the aluminium direct chill (DC) casting process. The variation of some key parameters that are known to influence the hot-tearing tendency is then studied. The results indicate that both liquid pressure drop due to feeding difficulties and tensile stress caused by thermal contraction of the solid phase are necessary for the formation of hot tears. Based upon results from the one-dimensional model, it is furthermore concluded that none of the hot-tearing criteria suggested in the literature are able to predict the variation in hot-tearing susceptibility resulting from a variation in all of the following parameters: solidification interval, cooling contraction of the solid phase, casting speed, and liquid fraction at coherency.

I. INTRODUCTION

HOT tearing is a problem commonly encountered in both ferrous and nonferrous castings. In aluminum direct chill (DC) casting, it is generally believed that hot tears start to develop in the mushy zone at a stage where the solid fraction is close to one.[1,2] The mushy zone is then definitely coherent, but continuous films of liquid still exist.[3] This distinguishes hot tears from cracks forming during the casting process after complete solidification (*e.g.*, References 4 and 5). It has also been established that the hot-tearing susceptibility increases with an increasing solidification interval[6,7] and with increased casting speed in the case of continuous or semicontinuous casting processes.[2] Singer and Cottrell[8] argued that the temperature range between dendrite coherency (where the material starts to develop strength) and the solidus temperature is of great importance with respect to hot-tearing characteristics.

Much effort has been put into the understanding of the hot-tearing phenomenon, and several hot-tearing theories have been proposed. Pellini[3] stated that hot tearing will result if the material is subjected to too high of an accumulated strain within the so-called vulnerable part of the solidification interval, whereas Guven and Hunt[9] and Campbell[1] also emphasized the role of tensile stresses in the formation of hot tears. Most hot-tearing criteria simply consider the size of the solidification interval,[1] stating that a long solidification range is associated with a larger hot-tearing susceptibility than a short range. Clyne and Davies[10] formulated a more refined such criterion based upon the time spent in different regimes of the solidification interval. They defined a vulnerable region in which thin continuous films of interdendritic liquid exist, and the permeability is low (volume fractions of solid in the range of 0.9 to 0.99). When thermal strains are induced in this region, the film is not able to sustain the stresses, and a hot tear will form. Feurer[11] focused on the pressure of the liquid present between the grains and argued that a hot tear will nucleate as a pore if the liquid is no longer able to fill the intergranular openings caused by the solidification shrinkage. Rappaz and co-workers[12,13,14] extended this approach to also take into account the feeding associated with tensile deformation of the solidified material in the direction transversal to the columnar dendritic growth. It is referred to Sigworth[15] for a more detailed review on work related to hot tearing.

In the cited literature, solidification shrinkage leading to interdendritic melt flow is one of the mechanisms associated with hot tearing. The other important mechanism is thermally induced deformation caused by the nonuniform cooling contraction of the casting. Closely linked to the latter mechanism are the constraints on the kinematic behavior imposed by the entirely solidified material close to the mushy zone. The interaction between, and relative importance of, these two mechanisms have, however, not yet been generally systematized in a mathematical model. This motivates for the present study directed towards the formulation of a two-phase model of an isotropic mushy zone in which both the solid and liquid phases are free to move and interact. The model is based upon the volume-averaged conservation equations as formulated by Ni and Beckermann,[16] and the main focus is on the coherent part of the solidification interval. It should be pointed out that the present work does not intend to present a new hot-tearing theory but instead a two-phase model of the mushy zone where quantities generally believed to be associated with hot tearing can be computed and compared. In this way, the model will shed some new light on the different hot-tearing criteria; both the ones formulated in terms of the liquid pressure as well as the ones formulated in terms of stress or strain.

In Section II, the general mathematical framework is derived, Section III is devoted to a simple stationary one-dimensional problem, and existing hot-tearing criteria are discussed in light of the new modeling results. Some basic assumptions of the new model along with the need for experimental input and more sohpisticated constitutive modeling are finally discussed in Section IV.

IVAR FARUP, Associate Professor, and ASBJORN MO, Professor, are with SINTEF Materials Technology, N-0314 Oslo, Norway.

Manuscript submitted April 12, 1999.

II. MATHEMATICAL MODEL

The mathematical model is based upon the general framework for volume-averaged conservation equations as presented by Ni and Beckermann.[16] The presentation is divided into three parts. First, the conservation equations are introduced and simplified. Then, the rheology of the solid phase is discussed. This is the most crucial part of the modeling work. Finally, miscellaneous simplified constitutive equations are listed. Most of them are chosen for simplicity and could easily be changed without introducing fundamental changes to the model.

A. *Conservation of Mass, Momentum, and Energy*

The equations for conservation of mass can be used directly on the form presented in Reference 16:

$$\frac{\partial(g_s\rho)}{\partial t} + \nabla \cdot (g_s\rho_s\mathbf{v}_s) = \Gamma \qquad [1]$$

$$\frac{\partial(g_l\rho_l)}{\partial t} + \nabla \cdot (g_l\rho_l\mathbf{v}_l) = -\Gamma \qquad [2]$$

where g_k represents the volume fraction of phase k ($k = s$ and l for solid and liquid, respectively), ρ_k denotes mass density, $\mathbf{v}_k$ is velocity, and Γ is the interfacial mass transfer due to phase change. It should be noted that adding the two conservation equations under the assumptions of

(1) constant density in the liquid and
(2) no pore formation, *i.e.*, $g_l + g_s = 1$

yields

$$-(\rho_s - \rho_l)\frac{\partial g_s}{\partial t} - g_s\left(\frac{\partial}{\partial t} + \mathbf{v}_s \cdot \nabla\right)\rho_s = \rho_l\nabla \cdot (g_l\mathbf{v}_l) + \rho_s \nabla \cdot (g_s\mathbf{v}_s) \qquad [3]$$

This shows that both solidification shrinkage (first term on left hand side) and cooling contraction (last term on left hand side) generally can contribute to sink/source terms (right hand side) for both the solid and liquid phases. Equation [3] does not however, link the two driving forces on the left hand side specifically to any of the two phases.

Before introducing the general volume-averaged energy and momentum equations, the following additional simplifications are introduced.[16]

(1) There is thermal equilibrium within the averaging volume.
(2) The enthalpy is a function of temperature only due to incompressible medium and low concentration of alloying elements.
(3) The dispersion fluxes are neglected.
(4) The specific heat capacity is constant within each phase.
(5) The momentum transfer due to phase change is neglected.

Relating the heat flux to the temperature by Fourier's law and adding the two energy equations for the solid and liquid phases then lead to

$$(g_s\rho_sC_s + g_l\rho_lC_l)\frac{\partial T}{\partial t} + (g_s\rho_sC_s\mathbf{v}_s + g_l\rho_lC_l\mathbf{v}_l) \cdot \nabla T = \nabla \cdot [(g_s\lambda_s + g_l\lambda_l)\nabla T] + L\Gamma \qquad [4]$$

Here, C_k is the heat capacity of phase k, λ_k is the heat conductivity, T is the temperature, and L is the latent heat. According to the discussion in Reference 17, the momentum transfer in liquid due to acceleration is negligible in a coherent mushy zone. For thermally induced deformations in the solid, this is clearly also the case. The momentum balance can then be expressed by

$$\bar{p}_{ki}\nabla g_k - \nabla(g_kp_k) + \nabla \cdot (g_k\boldsymbol{\sigma}'_k) + \mathbf{M}^d_k + g_k\rho_k\mathbf{g} = 0 \qquad [5]$$

where p_k is the pressure of phase k, $\boldsymbol{\sigma}'_k$ is the deviatoric stress tensor ($\mathrm{tr}\boldsymbol{\sigma}'_k = 0$), $\mathbf{M}^d_k$ is the interfacial transfer of momentum due to dissipative forces, $\mathbf{g}$ is the acceleration of gravity, and $\bar{p}_{ki}$ is the average interfacial pressure of phase k. The total volume averaged stress tensor of phase k is related to the pressure and the deviatoric stress tensor as

$$\boldsymbol{\sigma}_k = \boldsymbol{\sigma}'_k - p_k\mathbf{I} \qquad [6]$$

where $\mathbf{I}$ is the identity tensor.

In the liquid phase, $\bar{p}_{li} = p_l$ because of instantaneous pressure equilibration locally. Furthermore, at small liquid fractions, diffusion of momentum in the liquid phase is negligible compared to the momentum transfer due to dissipative interfacial forces. This simplifies the momentum equation for the liquid to

$$-g_l\nabla p_l - \mathbf{M} + g_l\rho_l\mathbf{g} = 0 \qquad [7]$$

where $\mathbf{M} = \mathbf{M}^d_s = -\mathbf{M}^d_l$ has been introduced. This simplified form of the liquid momentum equation has also been argued for by means of dimensional analysis in Reference 17.

For the solid pressure, it cannot always be assumed that $\bar{p}_{si} = p_s$ because an additional pressure can be transmitted through the coherent solid structure.[16] One can, however, assume mechanical equilibrium on the solid-liquid interface like in Reference 18, *i.e.*, assume that $\bar{p}_{si} = p_l$. It is implicit in this assumption that the surface tension is neglected. The resulting solid momentum equation reads

$$p_l\nabla g_s - \nabla(g_s\,p_s) + \nabla \cdot (g_s\boldsymbol{\sigma}'_s) + \mathbf{M} + g_s\rho_s\mathbf{g} = 0 \qquad [8]$$

B. *Rheology of the Solid Phase*

Above coherency, the solidified grains are assumed to move freely in the liquid, and it can be assumed that the pressure is equal in the two phases, $p_s = p_l$.[18] Mechanically, this means that the solid structure poses no restriction against isotropic compression/densification, *cf.*, the left hand part of Figure 1, and that the effects upon the momentum transfer of collisions and agglomeration are negligible. It should be noted that this does not necessarily mean that the velocities of the two phases are the same because the solidified grains can settle due to differences in density.

For the coherent part of the solidification interval (right hand side of Figure 1), this assumption is not valid because an additional pressure can be transmitted through the solid phase. In the present work, it will be assumed that the coherent network is connected in a manner such that the thermal contraction of the solid phase must be compensated for solely by deformation of the solid structure. In other words, the solid skeleton is assumed to be incompressible below the coherency temperature. In order to represent this in the present mathematical framework, Eq. [1] can be rewritten on the form

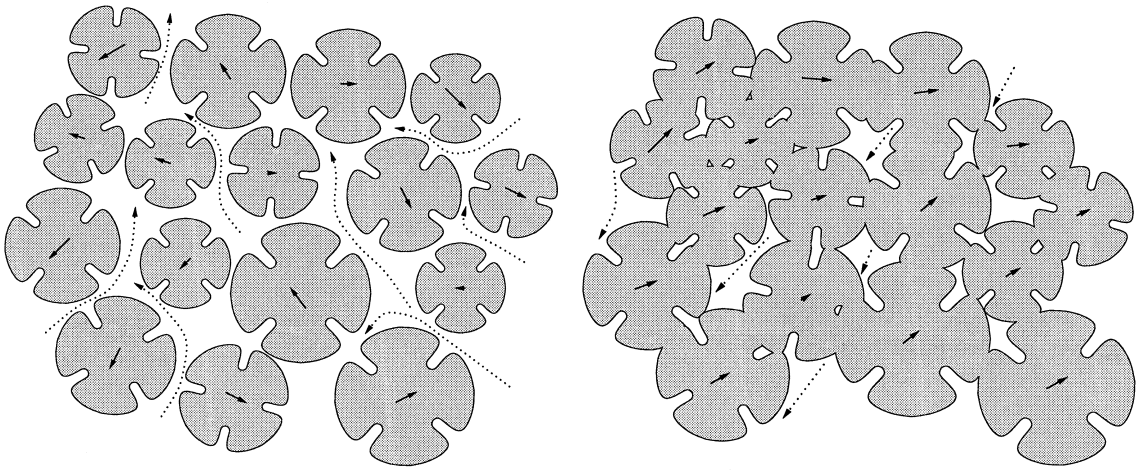

Fig. 1—Left: material above coherency, where $p_s = p_l$. Right: material below coherency, where $\partial\rho_s/\partial t + \nabla \cdot (\rho_s v_s) = 0$. The solid arrows indicate motion of the solid structure, whereas the dashed arrows indicate liquid flow.

$$g_s\left(\frac{\partial \rho_s}{\partial t} + \nabla \cdot (\rho_s \mathbf{v}_s)\right) + \rho_s \frac{Dg_s}{dt} = \Gamma \qquad [9]$$

where the material derivative, $Dg_s/dt = \partial g_s/\partial t + \mathbf{v}_s \cdot \nabla g_s$, has been introduced. Incompressibility means that the solid fracion can change only due to interfacial mass transfer. Mathematically, this means that

$$\rho_s \frac{Dg_s}{dt} = \Gamma \qquad [10]$$

which inserted into Eq. [9] leads to

$$\frac{\partial \rho_s}{\partial t} + \nabla \cdot (\rho_s \mathbf{v}_s) = 0 \qquad [11]$$

Thus, the single-phase continuity equation for the solid phase acts as a "closure equation" for the model.

These assumptions are in good agreement with the results reported by Pharr and Ashby,[19] *i.e.*, that creep in a coherent system is a result of deviatoric stress only and is not affected by the pressure in the two phases. The assumption is believed to be reasonable in the region close to the solidus where hot tearing is supposed to occur, although obviously not valid for solid fractions close to coherency.

In the (coherent) mushy zone, the thermally induced deformations (which according to Eq. [11] are assumed to take place in the solid phase only) are taken to be inelastic. The volume-averaged viscoplastic strain rate in the solid phase is then related to the gradient of the volume averaged solid velocity by

$$\boldsymbol{\epsilon}_s = \frac{1}{2}\left(\nabla \mathbf{v}_s + [\nabla \mathbf{v}_s]^T\right) - \frac{1}{3}\mathbf{1}\nabla \cdot \mathbf{v}_s \qquad [12]$$

The material is assumed to be isotropic, and $\boldsymbol{\epsilon}_s$ can thus be related to the deviatoric stress tensor by the Levy–Mises flow law:

$$\frac{\boldsymbol{\epsilon}_s}{\bar{\epsilon}_s} = \frac{3\boldsymbol{\sigma}'_s}{2\bar{\sigma}_s} \qquad [13]$$

where the effective solid strain rate and stress are defined as

$$\bar{\epsilon}_s = \sqrt{\frac{2}{3}\,\boldsymbol{\epsilon}_s : \boldsymbol{\epsilon}_s} \qquad [14]$$

$$\bar{\sigma}_s = \sqrt{\frac{3}{2}\,\boldsymbol{\sigma}'_s : \boldsymbol{\sigma}'_s} \qquad [15]$$

respectively.

Several authors have measured the rheological behavior in partially solidified aluminium alloys (*e.g.*, References 8 and 20 through 28). In most of these references, the mushy zone is considered as a single-phase system for which the effective stress, $\bar{\sigma}$, is related to the effective strain rate, $\bar{\epsilon}$, by a creep law on the form $\bar{\sigma} = F(\bar{\epsilon})$ with temperature-dependent parameters. In order to incorporate such a creep law into the present two-phase model, the single-phase variables associated with the experiments must be interpreted in terms of two-phase quantities used in the present model.

In the type of rheological measurements cited previously, there are approximately homogeneous deformation conditions in the sample, and the temperature and solid fraction are kept constant. It is, therefore, reasonable to assume that the volume-averaged velocities of the two phases are equal. This means that the measured single-phase strain rate as well as the solid and liquid strain rates in the sample all are the same. It is furthermore reasonable to assume that it is mainly the deformation of the solid phase that contributes to the measured stress in the coherent mushy sample, at least at solid fractions close to one. The single-phase effective strain rate, $\bar{\epsilon}$, associated with the measurements can thus be interpreted as the effective value of the volume averaged solid strain rate, $\bar{\epsilon}_s$.

According to the assumption of an incompressible solid skeleton in the coherent regime, only the deviatoric parts of the solid and liquid stress tensors contribute to deformation of the sample. The deviatoric single-phase stress tensor, $\boldsymbol{\sigma}'$, associated with the experimental measurements is furthermore related to the two-phase stresses by

$$\boldsymbol{\sigma}' = g_s\boldsymbol{\sigma}'_s + g_l\boldsymbol{\sigma}'_l \approx g_s\boldsymbol{\sigma}'_s \qquad [16]$$

Here, the approximation is introduced because the contribution from the liquid deviatoric stress tensor to $\boldsymbol{\sigma}'$ is negligible in rheological measurements carried out on coherent mushy samples. Combining this with the definition

$$\bar{\sigma} = \sqrt{\frac{3}{2}\,\boldsymbol{\sigma}' : \boldsymbol{\sigma}'} \qquad [17]$$

and Eq. [15], $\overline{\sigma}$ associated with the rheological measurements can be interpreted as $g_s\overline{\sigma}_s$. The creep law can now be written on the form

$$g_s\overline{\sigma}_s = F(\overline{\epsilon}_s) \qquad [18]$$

where the function F is the same as the one determined in experiments in which the mushy zone is considered as a single-phase system.

C. *Simplified Constitutive Equations*

Knowledge of the solid fraction can be obtained by modeling the solidification, Γ, *e.g.*, as in Reference 18, or by coupling to a more sophisticated microscopic grain growth model, *e.g.*, as in References 29 and 30. A simpler approach is to assume a unique solidification path. In the present study, where only binary alloys are considered, the lever rule,

$$g_l = \frac{\rho_s(c_0 - kc_l(T))}{c_0(\rho_s - \rho_l) - c_l(T)(\rho_l - k\rho_s)} \qquad [19]$$

will be used for simplicity. Here, $c_l(T) = (T - T_m)/m$, and $k = c_s/c_l$ is the partition coefficient. If the initial liquid concentration, c_0, is greater than the solvus, eutectic will form at the end of solidification

$$T = T_e \text{ when } 0 \le g_l \le g_e \qquad [20]$$

where g_e is the fraction of eutectic.

Because free convection in the liquid phase is beyond the scope of the present model, the liquid density is assumed to be constant. The solid density, on the other hand, is taken to be a known linear[16] function of the temperature alone:

$$\rho_s = \rho_l(1 + \beta_s)[1 + \beta_T(T - T_{\text{liq}})] \qquad [21]$$

where $\beta_s = [\rho_s(T_{\text{liq}}) - \rho_l]/\rho_l$ represents the solidification shrinkage, $\beta_T = [\rho_s(T)/\rho_s(T_{\text{liq}}) - 1]/(T - T_{\text{liq}})$ is the cooling contraction of the solid phase, and T_{liq} is the liquidus temperature.

The momentum transfer between the solid and liquid phases due to dissipative interfacial forces is assumed to follow Darcy's law:

$$\mathbf{M} = g_l^2\mu(\mathbf{v}_l - \mathbf{v}_s)/K(g_l) \qquad [22]$$

where μ is the viscosity of the liquid. In the present study, $K(g_l)$ is modeled by the permeability given by the Kozeny–Carman relation:[31]

$$K = K_0 g_l^3/(1 - g_l)^2 \qquad [23]$$

where $K_0 = 1/(5S^2)$. The variable S is the specific solid-liquid interface area. Following Asai and Muchi,[32] it is assumed that $S = 6/D$, where D is the secondary dendrite arm spacing that is taken as a constant in the present work.

The stress-strain relationship, *i.e.*, the function F in Eq. [18] is often chosen as a pure power law:[20]

$$g_s\overline{\sigma}_s = k\overline{\epsilon}_s^n \qquad [24]$$

where the parameters k and n should be taken as functions of g_s or T. The values for the effective stress at a given solid fraction in the mushy zone found in the literature varies from ~20 kPa in References 8 and 26 to ~1 MPa in References 20 and 23. However, all the measurements show that the strength decreases quite rapidly from the solidus temperature to coherency. Based upon these observations, the following *ad hoc* expressions have been chosen for the creep law parameters for $0 \le g_l \le g_{l,\text{coh}}$, where $g_{l,\text{coh}}$ is the liquid fraction at coherency,

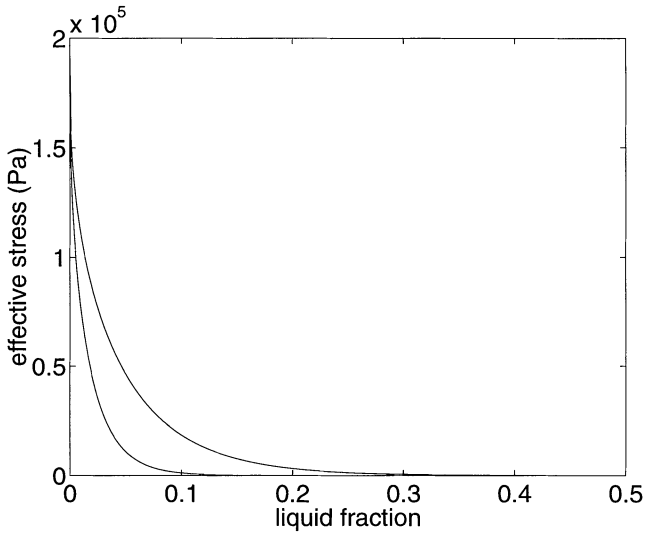

Fig. 2—Effective stress given by the creep power law for an effective strain rate $\overline{\epsilon} = 10^{-4}$ s^{-1} for $g_{l,\text{coh}} = 0.5$ and $g_{l,\text{coh}} = 0.2$ as a function of the liquid fraction.

$$n = n_0 + (1 - n_0)\left(\frac{g_l}{g_{l,\text{coh}}}\right) \qquad [25]$$

$$k = k_0 - k_0\left(\frac{g_l}{g_{l,\text{coh}}}\right)^{0.25} \qquad [26]$$

The linear dependance of n upon g_l is in agreement with the results of Drezet and Eggeler.[20] The expression for k was subsequently obtained by fitting $\overline{\sigma}(g_l)$ for a given strain rate in order to obtain qualitative agreement with the results given in Reference 26 (*cf.* Figure 2). For $g_l \ge g_{l,\text{coh}}$, the stress in the solid phase is neglected.

III. ONE-DIMENSIONAL TEST PROBLEM

Consider the one-dimensional stationary Bridgmanlike casting process sketched on the left hand side of Figure 3. At the bottom ($x = a$), where the material is entirely solidified with temperature $T = T_{\text{sol}}$, solid material is taken out at a constant casting speed, V. Melt with temperature $T = T_{\text{liq}}$ flows into the domain at the top ($x = 0$). Due to solidification shrinkage and cooling contraction of the solid phase, the vertical liquid velocity at the top is slightly higher than the casting speed. It is assumed that all transport phenomena occur in one direction only, *viz.*, along the axis of solidification. This means, in addition to no heat extraction in the horizontal direction, that the contracting material is restricted from contracting horizontally. Thus, stress will arise trying to tear the material apart along the axis. It is assumed that the gravity, **g**, can be neglected because the contribution of the weight of the liquid metal to the liquid pressure is negligible in the bottom of the mushy zone. It should be noted that this makes the assumption of equal pressures of the two phases above coherency even more appropriate because it

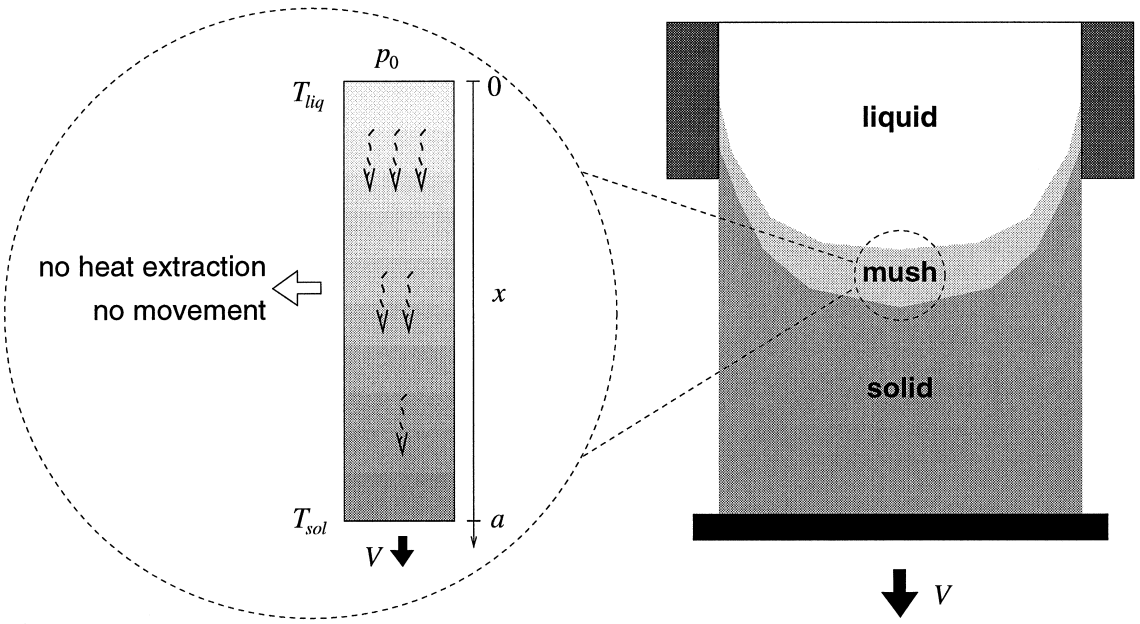

Fig. 3—Simplified one-dimensional test problem and its relevance for the DC casting process.

means that no settling of freely floating grains (or agglomoration of grains) will take place. It is furthermore assumed that the pressure of the surroundings is zero. This only means that the calculated pressure will be relative to the ambient pressure such that a negative value denotes a pressure lower than the atmospheric pressure. For this case, the model presented in the previous section has been simplified in Appendix A and implemented numerically in MATLAB* using the finite difference method as outlined in Appendix B.

*MATLAB is provided by Computer Solutions Europe (Trondheim, Norway) AB (COMSOL) under an academic license.

It should be noted that this simple stationary one-dimensional test problem has several analogies to the situation in the center of a DC casting process where the mushy zone is restricted to move in the vertical direction due to the presence of a solidified shell surrounding the solidifying region. Furthermore, if the sump is not too deep and curved in the center heat extraction mainly occurs along the axis.

Table I. Input Parameters to the Model for the Default Case

$V = 10^{-3}$ m/s	casting speed
$a = 10^{-2}$ m	length of mushy zone
$M = 5000$	number of nodes
$p_0 = 0$	metallostatic pressure
$k_0 = 2 \cdot 10^6$	creep law constant
$n_0 = 0.25$	creep law constant
$g_{l,\mathrm{coh}} = 0.5$	liquid fraction at coherency
$\beta_s = 0.0658$	solidification shrinkage
$\beta_T = -9 \cdot 10^{-5}$ K^{-1}	thermal expansion
$c_0 = 0.045$	concentration of Cu
$c_e = 0.33$	concentration at eutectic
$k = 0.17$	partition coefficient
$m = -339$ K	slope of liquidus line
$T_{mp} = 933$ K	melting temperature (pure Al)
$T_e = 821$ K	eutectic temperature
$C_l = 1060$ J/(kg K)	specific heat in liquid
$C_s = 1060$ J/(kg K)	specific heat in solid
$\lambda_l = 83$ W/(m K)	heat conductivity in liquid
$\lambda_s = 192$ W/(m K)	heat conductivity in solid
$L = 4 \cdot 10^5$ J/kg	latent heat

A. *Default Case*

The one-dimensional equations have been solved for an Al4.5%Cu alloy under conditions relevant for the DC casting process. The parameters given as input to the model for this case are listed in Table I. It should be noted that parameters related to the solidification characteristics as well as to the mechanical behavior are necessary input to the model. Results from running the model with these parameters are shown in Figure 4.

The temperature profile shown in Figure 4(a) is almost linear. This is the case as long as the casting speed is low. By increasing the casting speed, the terms for convection and latent heat release in the energy equation become increasingly important. The temperature profile then becomes more curved with a higher temperature gradient close to the solidus. The solid fraction shown in Figure 4(b) is related directly to the temperature by the lever rule (Eq. [19]). It should be noted that its curved shape causes the major part of the mushy zone to be coherent even when $g_{l,\mathrm{coh}}$ is as high as 0.5.

Figure 4(c) shows the volume-averaged velocities of the solid and liquid phases. In the region above the coherency, *i.e.*, where $g_l > g_{l,\mathrm{coh}}$, the solidified grains float freely in the liquid with the same velocity as the liquid due to the fact that gravity is neglected (*cf.* Eq. [A.7]). At coherency, the floating grains bump into the coherent solid phase, causing a rapid change in velocity. The rapid change in velocity is a consequence of the assumption that the mushy zone behavior changes abruptly at the coherency point. It

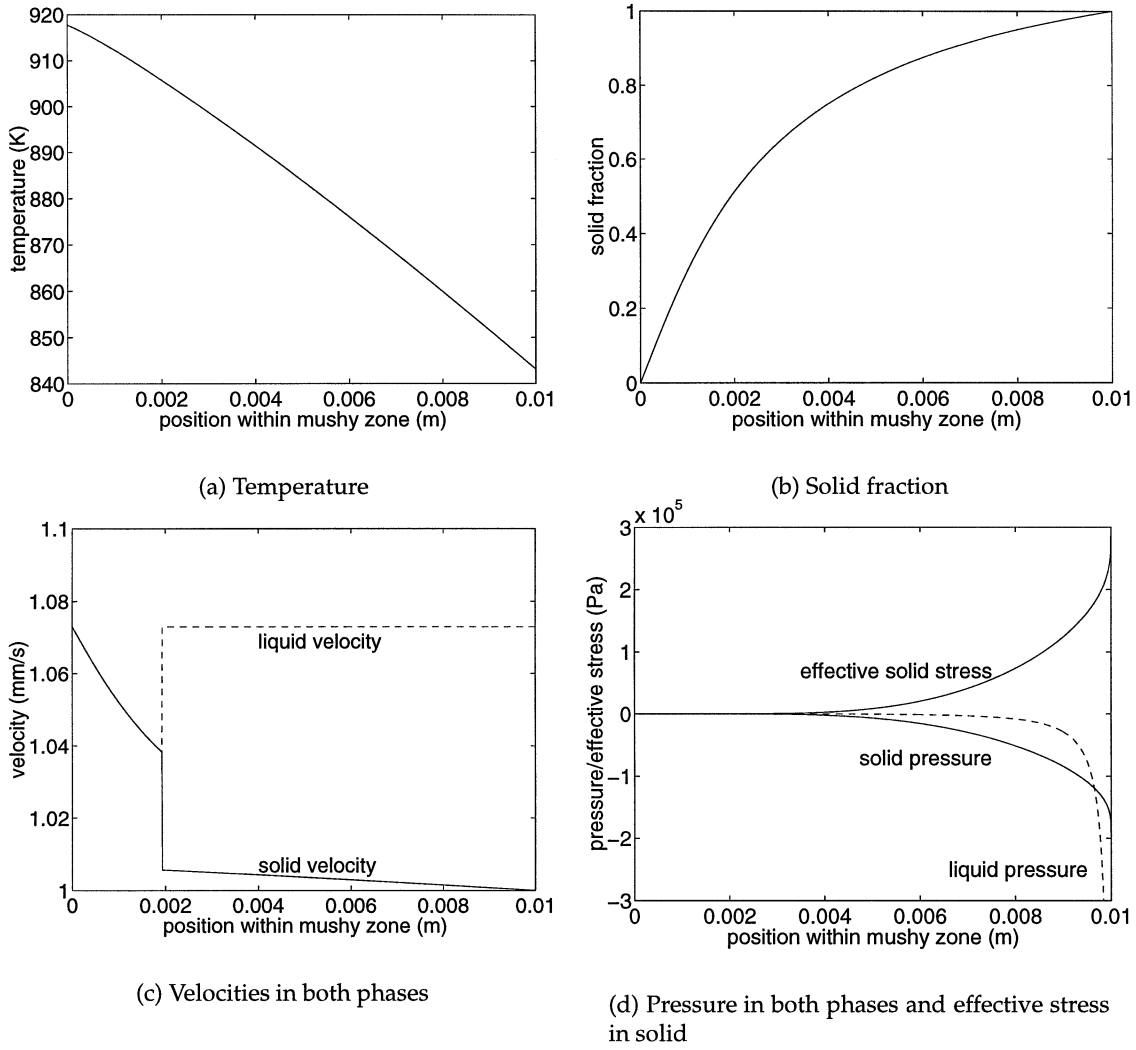

Fig. 4—(*a*) through (*d*) Results from running the model on the default case. Every quantity is plotted as a function of the position within the mushy zone.

turns out as a consequence of the conservation equations that the liquid velocity is constant in the coherent range (*cf.*, Eq. [A.6]).

Figure 4(d) shows the stress and pressure. The upper curve shows the effective stress in the solid phase, which decreases rapidly from its value at the solidus to zero at coherency. The absolute values of the pressures in the solid and liquid phases show a similar behavior. In the region in the mushy zone where hot tears might form, *i.e.*, at liquid fractions between 0.01 and 0.1, the liquid pressure is lower than the solid pressure. It is therefore reasonable to argue that hot tears do not form as a consequence of hydrostatic depression alone (although pore formation might be the result of the low liquid pressure). Tensile stress is also required, as pointed out by Campbell.[1] In the present situation, the stress in the directions transversal to the casting direction is indeed tensile because the pressure of the solid phase is negative (*i.e.*, smaller than the ambient pressure), and the contribution from the deviatoric stress tensor is tensile (*cf.*, Eqs. [6] and [A.12]).

B. *Parameter studies*

The hot-tearing susceptibility is known to depend critically upon the solidification interval,[10,12] the thermal contraction of the solid phase,[3] the liquid fraction at coherency,[8] and, in the case of DC casting, the casting speed.[2] Case studies in which these four parameters are varied have therefore been performed. Because variations in these parameters affect the hot-tearing tendency, they should result in variations in key parameters, *e.g.*, stress and pressure, in the present model.

If the hot-tearing susceptibility is, as suggested in References 11 and 12, related to the liquid pressure drop, variations in these parameters should be reflected in the calculated liquid pressure. For the default case, the liquid pressure (dashed line in Figure 4(d)) becomes increasingly small as the solid fraction tends toward one. This is because there is no formation of eutectic (lever rule is applied, and the concentration is just below the solvus), the permeability is zero for a fully solidified material, and no pores are allowed to form in the present model. It is, therefore, more instructive

to study the values of the pressure and stress at a critical point in the mushy zone, which according to empirical observations has a high hot-tearing susceptibility. Following Clyne and Davies,[10] this is taken to be where $g_l = 1$ pct when there is no formation of eutectic, or the fraction of the eutectic is smaller than 1 pct. When the eutectic fraction is larger than 1 pct, the growing plane eutectic front is referred to as the critical point within the mushy zone (*cf.*, Reference 12).

1. *Alloy Composition/Solidification Interval*

Varying the composition of the alloy results in variations in the solidification interval by Eq. [19]. Figure 5 shows the effect of varying the amount of copper in the binary Al-Cu alloy on the liquid pressure at the critical point (as defined previously) under otherwise identical casting conditions. The so-called lambda curve (*e.g.*, References 1–10, and 12) is reproduced, indicating a peak in the pressure for a certain alloy composition at which hot tearing is most likely to occur. This is similar to the results obtained by Campbell[33] for the determination of pore formation in castings. The effective stress and pressure in the solid phase is, on the other hand, not affected by the variation in composition because it is mainly a function of the cooling rate. This indicates that a sufficient drop in the liquid pressure can be associated with the formation of hot tears.

The alloy composition at the peak corresponds to the composition giving a maximum solidification interval. For concentrations higher than the peak, the formation of eutectic leads to a rapid decrease in the pressure drop. In this modeling case, it occurs at quite a high concentration of copper because the lever rule is applied for describing the solidification path. If, instead, a model with limited or no back diffusion were applied, the peak would occur at a lower concentration of copper because more eutectic would form. From experimental work, it is known that Al-Cu alloys containing approximately 0.5 to 2 pct of copper are the ones most susceptible to hot tearing.[6,7,34]

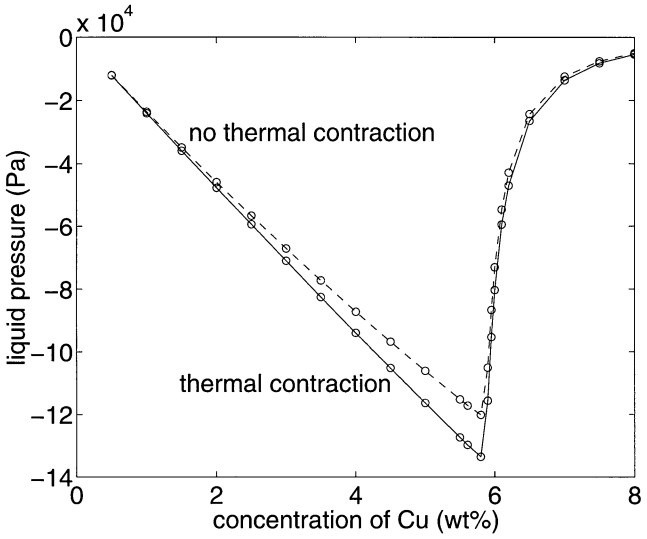

Fig. 5—Liquid pressure at the critical position in the mushy zone as a function of composition in a binary Al-Cu alloy for otherwise identical casting conditions (solid line) and for the same system with no cooling contraction of the solid phase (dashed line).

The lambda curve is reproduced by the criteria of Rappaz *et al.*[12] and Clyne and Davies.[10] A lambda like curve would also be the result if the accumulated strain in the coherent mushy zone was considered as a function of alloy composition. This is because of the dependency of the solidification interval upon the alloy composition. The viscoplastic strain rate, on the other hand, does not vary significantly when varying the alloy composition. A criterion based solely upon this quantity would, therefore, not be able to reproduce a lambda-like curve, and, thus, not reflect the dependency of the hot-tearing susceptibility upon the alloy composition.

2. *Cooling Contraction*

When the same numerical experiment is performed on an artificial alloy that is similar to the Al-Cu system in all respects except that there is no cooling contraction of the solid phase ($\beta_T = 0$); nearly the same result is obtained in terms of the liquid pressure (dashed line in Figure 5). In this alloy, there is obviously no thermally induced stress or strain in the solid phase whatsoever. One would not, therefore, expect hot tearing[1] but instead porosity formation. A hot-tearing criterion based upon the liquid pressure would, on the other hand, predict almost the same hot-tearing susceptibility for the two cases. This indicates that the liquid pressure drop cannot constitute the full basis for a hot-tearing criterion.

By comparing the evolution of the solid fraction *vs.* time, it is found that the criterion due to Clyne and Davies[10] would give the same hot-tearing susceptibility for this case as for the one including thermal contractions of the solid phase. This also applies for criteria formulated solely in terms of the liquid pressure, as shown here. On the other hand, criteria formulated in terms of the accumulated strain or the strain rate in the mushy zone, like, *e.g.*, the one proposed in References 2 and 12, would obviously give different susceptibilities for the two cases because the viscoplastic strain is induced by the cooling contraction of the solid phase.

3. *Casting Speed*

When varying the casting speed, *V*, the effective stress in the solid phase and the pressure in both phases at the critical point varies, as shown in Figure 6. It is seen that the liquid pressure at the critical point decreases rapidly with increasing casting speed until a certain point where the effect suddenly stops. This is when the terms for convection and release of latent heat become dominating in the energy equation.* It is also observed that the negative solid pressure and the effective stress of the solid phase are increasing with increasing speed. This is in agreement with models for thermally induced deformations in DC casting (*e.g.*, Reference 35).

*In a real DC casting situation, this effect would probably be less emphasised because, at high casting speed, the sump profile is quite deep and strongly curved. Then, the assumptions made in the present model concerning one-dimensionality are no longer applicable for the heat flow.

Results from the one-dimensional model reveal that the total accumulated viscoplastic strain is almost the same for

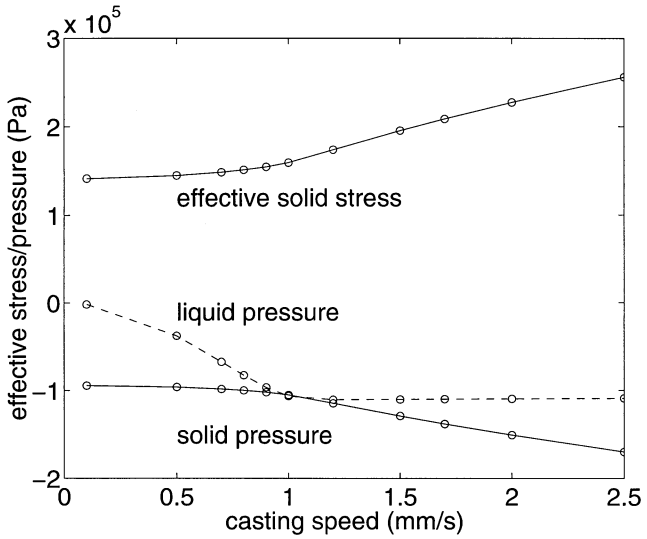

Fig. 6—The effect of the casting speed on effective stress in the solid phase and on the pressure in both phases at the critical point within the mushy zone.

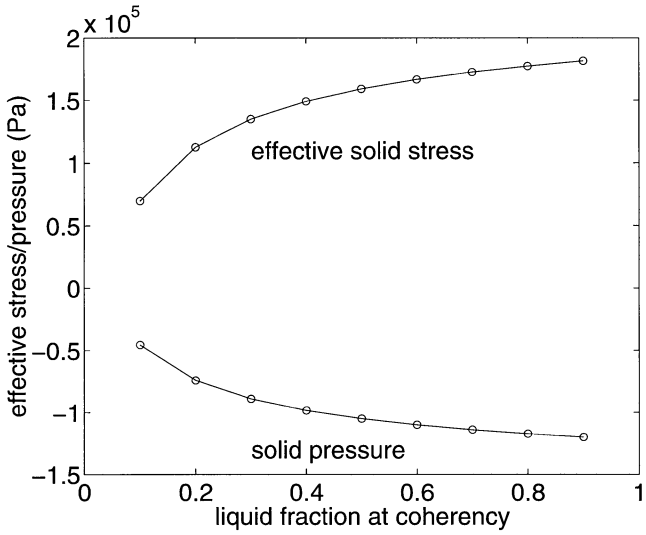

Fig. 7—The effect of the liquid fraction at coherency, $g_{l,\mathrm{coh}}$, on pressure and effective stress of the solid phase at the critical point within the mushy zone.

any casting speed. This is because the total cooling contraction of the solid phase is given by the difference in temperature between coherency and solidus. In a three-dimensional case, this would not necessarily be the case because the viscoplastic strain is induced by the inhomogeneity of the thermal contractions. However, it should still be noted that criteria based upon the total accumulated strain, *e.g.*, like in Reference 3, cannot predict the increase in hot-tearing susceptibility by casting speed in this case study. The same is found to apply for the hot-tearing criterion of Clyne and Davies[10] by comparing the evolution of solid fraction *vs* time because their criterion is based upon the relative amount of time spent in different regimes of the solidification interval. The viscoplastic strain rate, on the other hand, increases with increasing casting speed (*cf.*, Figure 6 and Eq. [24]), so criteria based upon this parameter, *e.g.*, Reference 12, will predict increased susceptibility for the present case study. The same applies to criteria formulated in terms of the liquid pressure.

4. *Liquid Fraction at Coherency*

An input parameter to the model is the value of the liquid fraction at coherency, $g_{l,\mathrm{coh}}$. According to experiments, an increase in this value leads to an increased hot-tearing susceptibility. However, it turns out that the liquid pressure at the critical point is completely unaffected by this variation in the liquid fraction at coherency. This is because the negative liquid pressure builds up very near the end of solidification and is almost unaffected of at which position in the mushy zone it starts building up. Thus, a hot-tearing criterion formulated in terms of the liquid pressure alone will not reflect the effect of a variation in the liquid fraction at coherency.

On the other hand, Figure 7 shows that the liquid fraction at coherency has a strong impact upon the stress and pressure in the solid phase. This is because coherency at a high liquid fraction gives rise to a large coherent solidification range in which stress can build up in the solid phase. It is, therefore, reasonable to argue that a theory for hot tearing must include the stress buildup in the solid phase.

Again, the different attempts toward formulating a hot-tearing criterion can be compared. From the present results, it is clear that a criterion formulated in terms of the liquid pressure would not predict any variation when varying the liquid fraction at coherency. Also, criteria based upon the viscoplastic strain rate in the coherent part of the mushy zone would be unaffected by a shift in the liquid fraction at coherency because the viscoplastic strain rate is unaffected in the region close to the solidus. Thus, the criterion in Reference 12 would also fail. Criteria based upon the total accumulated strain would, on the other hand, predict an increased hot-tearing susceptibility with increasing coherent interval because the strain accumulates over a wider temperature range. The solidification characteristic does not vary significantly as a result of varying the liquid fraction at coherency so the criterion in Reference 10 would fail.

IV. DISCUSSION

By the parameter studies, the new two-phase model has been applied to compute the lambda curve, the stress buildup in the mushy zone, and how the liquid fraction at coherency quantitatively affects the stress in the solid phase. Several well-known empirical observations are, in other words, predicted by the new approach. In the case studies, it is also pointed out that the different existing hot-tearing criteria are able to qualitatively predict the variation in hot-tearing susceptibility when varying some of the critical process parameters. However, none of the existing criteria are able to correctly predict the variation in hot-tearing tendency due to all parameter variations introduced. This result is summarized in Table II, and it clearly indicates the need for new and more sophisticated hot-tearing criteria and a theory upon which such criteria could be based.

It should, however, be noted that the table shows the ability of the proposed criteria to predict the change of hot-tearing susceptibility in the one-dimensional model problem, not generally. Some important aspects might therefore be lost. For example, in the one-dimensional case, the strain rate of the solid phase is given directly by the continuity equation without involving the momentum equation. Thus, the strain rate of the solid phase is independent of the

Table II. Summary of the Ability of Different Types of Hot-Tearing Criteria to Predict a Variation in Hot-Tearing Susceptibility upon Varying of Different Process Parameters

Type of Criterion	Alloy Composition	Thermal Contraction	Casting Speed	Liquid Fraction at Coherency
Strain rate	−	+	+	−
Accumulated strain	+	+	−	+
Liquid pressure	+	−	+	−
Clyne and Davies[10]	+	−	−	−
Rappaz *et al.*[12]	+	+	+	−

mechanical behavior of the mushy zone. In a real two- or three-dimensional situation, this would be different. A material with a low-strength mushy zone would have a higher strain concentration at the warmest locations than material with a mushy zone of higher strength, and, thus, the hot-tearing tendency would increase. Therefore, both the strength of the solid phase as well as the liquid fraction at coherency will be more important parameters in real multidimensional problems than in the present one-dimensional model problem. Consequently, the criterion of Rappaz *et al.*[12] might be affected by a change of coherency point through a corresponding change in mechanical behavior.

One of the most critical assumptions on which the new approach is based is that the coherent solid phase is connected in a manner such that the thermal contraction of the solid phase must be compensated for solely by deformation of the solid structure, *cf.*, Eq. [11]. In the temperature range close to coherency, this assumption is obviously not valid. Fortunately, this region is not of major interest because hot tears are known to form in the region very close to the solidus where the assumption is reasonable. It should, however, be kept in mind that calculated stress values in the solid phase close to the solidus will be affected by the incompressibility assumption because stress start to build up already at coherency. On the other hand, the model gives physically reasonable results even when incompressibility is assumed and some new insight in the phenomena underlying hot tearing can hopefully be gained.

In References 25, 36, and 37, a two-phase mathematical framework for a compressible and isothermal mushy zone was proposed. Unfortunately, it is not straight forward to generalize this to a situation with temperature change and solidification. First, the mechanism of thermal contraction in the region near the coherency point is not known. More specifically, it is not obvious whether grains contract independently or as a connected network. Secondly, no experimental determination of the rheology of compression for microstructural conditions relevant for casting processes is available.

Another challenge concerning the mushy zone rheology is that the majority of measurements has been directed toward semisolid forming rather than toward thermally induced deformation and hot tearing. These measurements are, therefore, performed with much higher strain rates and for a different microstructure than those relevant for the present study.

In the literature on hot tearing, it is pointed out that the liquid melt occurs as films around the grains or is trapped within isolated pockets during the last part of the solidification.[38] How a possible transition between these two flow regimes affects flow conditions and/or the rheological behavior of the mushy zone should, therefore, be addressed.

It has been suggested in the literature that hot-tear formation is closely related to porosity (e.g., Reference 12), and that pores may act as nucleation points for hot tears. It should be emphasised that models for pore formation during casting (*e.g.*, Reference 39) could be incorporated in the present mathematical framework by introducing a pore fraction (third phase) in addition to the solid and liquid phases. However, it is not obvious how the presence of pores would affect the rheological behavior of the solid-liquid system.

In Section II–C, it was noted that the mathematical framework presented could be coupled to models for solidification with grain growth including microstructure evolution. If this is done, it would, in principle, be possible to introduce more sophisticated models for the material behavior taking the present microstructure into account. However, such an approach requires more research on the effect of coalescence, *i.e.*, solid bridging between different grains. Also, the microstructure evolution near the end of solidification and the effect of impingement of neighboring growing grains on the mechanical properties should be addressed.

V. CONCLUSIONS

A two-phase continuum model for an isotropic mushy zone is presented. In this model, after-feeding of the liquid melt due to solidification shrinkage is taken into account as well as thermally induced deformation of the solid phase. Results from a one-dimensional model problem reveals

1. The pressure in the solid phase is higher than the pressure in the liquid phase close to the end of solidification. This indicates that tensile stress is necessary for the formation of hot tears.
2. The so-called lambda curve is reproduced for the liquid pressure *vs* alloy composition. This indicates that feeding difficulties is important for the formation of hot tears.
3. The liquid pressure is more or less unchanged for an artificial alloy with no cooling contraction in the solid phase. This indicates that a liquid pressure drop above some critical value cannot be the only parameter in a hot-tearing criterion.
4. Increasing the casting speed has a great impact on stress and pressure in both the solid and liquid phases.
5. A variation in the liquid fraction at coherency does not affect the liquid pressure, whereas it is of major importance for the stress and pressure in the solid phase.
6. None of the hot-tearing criteria suggested in the literature

are able to predict the variation in hot-tearing susceptibility resulting from a variation in all of the following parameters: solidification interval, cooling contraction of the solid phase, casting speed, and liquid fraction at coherency.

ACKNOWLEDGMENTS

The authors thank Dr. Håvard J. Thevik, Department for Strategic Research, DNV (Oslo, Norway), for fruitful discussions and suggestions during the work. This research has been funded by Hydro Aluminium, Elkem Aluminium, Hydro Raufoss Automotive Research Centre, and the Research Council of Norway through the project PRO-SMAT-Støperikompetanse.

APPENDIX A

Mathematical model for one-dimensional test problem

For the stationary one-dimensional test problem, the partial differential equations of the previous section reduce to ordinary nonlinear ones ($\partial/\partial t = 0$). The energy Eq. [4] reads

$$(C_s g_s \rho_s v_s + C_l g_l \rho_l v_l) \frac{dT}{dx} = \frac{d}{dx}\left[(g_s \lambda_s + g_l \lambda_l) \frac{dT}{dx}\right] + L \frac{d}{dx}(g_s \rho_s v_s) \quad [A1]$$

Here, the one-dimensional continuity equation for the solid phase, Eq. [1], has been used for eliminating Γ.

Combining the continuity equations for the two phases, Eqs. [1] and [2] for this particular case, gives

$$\frac{d}{dx}(g_s \rho_s v_s + g_l \rho_l v_l) = 0 \quad [A2]$$

This equation can be integrated analytically using the boundary conditions at $x = a$, giving

$$g_s \rho_s v_s + g_l \rho_l v_l = \rho_s(T_{sol}) V \quad [A3]$$

For the coherent part of the mushy zone, the solid phase is assumed to obey the single-phase continuity equation, Eq. [11]:

$$\frac{d}{dx}(\rho_s v_s) = 0 \quad [A4]$$

which can be integrated together with the boundary conditions at $x = a$, giving

$$v_s(x) = \frac{\rho_s(T_{sol}) V}{\rho_s(x)} \quad [A5]$$

It is, thus, a one-to-one correspondence between the density and the velocity of the solid phase in the coherent region. It should be noticed that this is caused by the stationarity and the one-dimensionality of the process and is obviously not a general result. Inserting this value for the solid velocity into the continuity equation, Eq. [A3] shows that the liquid velocity in the coherent regime is constant:

$$v_l(x) = \frac{\rho_s(T_{sol}) V}{\rho_l} \quad [A6]$$

For the noncoherent region of the mushy zone, where the pressure is the same in the two phases, the momentum equations, Eqs. [7] and [8], give $v_s = v_l$ when the process is one-dimensional and without gravity. Inserting this into the continuity equation, Eq. [A3], gives

$$v_k(x) = \frac{\rho_s(T_{sol}) V}{g_s(x)\rho_s(x) + g_l(x)\rho_l} \quad [A7]$$

for $k = s, l$. The Eqs. [A1] and [A5] through [A7] can now be solved numerically in the entire mushy zone applying the lever rule (Eq. [19]) and the equation for the solid density, Eq. [21], yielding the temperature, solid fraction, density, and the velocities of both phases. It should be noted that in this one-dimensional case, like in one-dimensional computation of macrosegregation under certain conditions,[40] the velocities can be obtained without solving the momentum equations.

When the temperature, solid and liquid fractions, densities, and velocities of both phases are known, the pressure and stress can be determined using the momentum equations, Eqs. [7] and [8], and the constitutive relations, Eqs. [12] through [15] and [24] as follows.

The liquid pressure can be found by integrating the simplified one-dimensional version of the liquid momentum equation (which is reduced to Darcy's law by the neglect of gravity):

$$\frac{dp_l}{dx} = -\frac{1}{g_l} M \quad [A8]$$

The deviatoric strain rate of the solid phase can be found directly from the velocity. In dyadic notation (**i**, **j**, and **k** being unit vectors in the x, y, and z directions, respectively)

$$\nabla \mathbf{v}_s = v_s'(x)\mathbf{ii} \quad [A9]$$

$$\boldsymbol{\epsilon}_s = \frac{2}{3} v_s'(x)\left(\mathbf{ii} - \frac{1}{2}(\mathbf{jj} + \mathbf{kk})\right) \quad [A10]$$

$$\bar{\epsilon}_s = \frac{2}{3}|v_s'(x)| \quad [A11]$$

where the prime denotes differentiation with respect to x. With these expressions inserted, the Levy–Mises flow law (Eq. [13]) reduces to

$$\boldsymbol{\sigma}_s' = \frac{2\bar{\sigma}}{3} \frac{v_s'(x)}{|v_s'(x)|}\left(\mathbf{ii} - \frac{1}{2}(\mathbf{jj} + \mathbf{kk})\right) \quad [A12]$$

From this equation, it is clear that the contribution from the deviatoric stress tensor to the stress in the y and z directions will be tensile because $v_s'(x) < 0$, as already discussed. The effective solid stress, $\bar{\sigma}_s$, is found from the constitutive equation, Eq. [24]. This gives

$$g_s \boldsymbol{\sigma}_s' = \frac{2}{3} k(x)\left(\frac{2}{3}|v_s'(x)|\right)^{n(x)} \frac{v_s'(x)}{|v_s'(x)|}\left(\mathbf{ii} - \frac{1}{2}(\mathbf{jj} + \mathbf{kk})\right) \quad [A13]$$

and, thus,

$$\nabla \cdot (g_s \boldsymbol{\sigma}'_s) = \frac{2}{3}\frac{d}{dx}\left(k(x)\left(\frac{2}{3}\left|v'_s(x)\right|\right)^{n(x)}\frac{v'_s(x)}{\left|v'_s(x)\right|}\right) \quad [A14]$$

The pressure of the solid phase can now be found by adding the solid and liquid momentum equations, Eqs. [7] and [8] (neglecting the gravity term in agreement with the assumptions of the simplified model):

$$\frac{d}{dx}\left(g_l p_l + g_s p_s + \frac{2}{3} g_s \bar{\sigma}_s\right) = 0 \quad [A15]$$

and integrating, using that $p_s(x = 0) = 0$

$$p_s(x) = -\frac{1}{g_s(x)}\left(\frac{2}{3} g_s(x)\bar{\sigma}_s(x) + g_l(x)p_l(x)\right) \quad [A16]$$

APPENDIX B

Numerical solution procedure

In order to solve the system consisting of the heat equation, Eq. [A1] and the expressions for the velocities in both phases, Eqs. [A5], [A6], and [A7], the heat equation has been discretized using the finite difference method on a grid with equidistant nodes. In the convection term, upwind differences has been applied (*e.g.*, Reference 41), and for the terms where values between the nodes were needed, *e.g.*, for the value of $g_l\lambda_l + g_s\lambda_s$, simple arithmetic middles were used. It was also found necessary to treat the term for release of latent heat partly implicitly in order to obtain numerical stability. This means that the term was rewritten according to

$$\frac{d}{dx}(g_s\rho_s v_s) = g_s\frac{d}{dx}(\rho_s v_s) + \rho_s v_s\frac{dg_s}{dT}\frac{dT}{dx} \quad [B1]$$

where the factor dg_s/dT is determined numerically.

The resulting discretized energy equation is nonlinear because it contains the temperature dependent fractions and densities of the two phases. The equation is, therefore, solved by simple iteration using the values from the previous iteration in the nonlinear terms. A starting point for the iteration is found from the analytical solution of the energy equation with

$$\rho_s = \rho_l = \text{const} \quad [B2]$$

$$v_s = v_l = V = \text{const} \quad [B3]$$

$$C_s = C_l = \text{const} \quad [B4]$$

$$\lambda_s = \lambda_l = \text{const} \quad [B5]$$

which is straight forwardly found to be

$$T(x) = T_{\text{sol}} + \frac{T_{\text{liq}} - T_{\text{sol}}}{\exp\left(-C_l V \rho_l a/\lambda_l\right) - 1}\left[\exp\left(C_l V \rho_l (a - x)/\lambda_l\right) - 1\right] \quad [B6]$$

From this, the initial guess, the solid fraction is determined by the lever rule (Eq. [19]), the solid density by Eq. [21], and the velocities by Eqs. [A5], [A6], and [A7]. With these values inserted, the energy equation is solved by the finite difference method, and this process is repeated until

$$\max\left(\frac{|T - \bar{T}|}{T_{\text{liq}} - T_{\text{sol}}}\right) + \frac{\max|v_s - \bar{v}_s|}{\max|v_s - V|} < 10^{-4} \quad [B7]$$

where the barred variables refer to the values of the corresponding variables at the previous iteration step. The last term and the low tolerance have been applied in order to obtain a sufficiently accurate description of the liquid pressure close to the solidus.

The scheme has been implemented in MATLAB, and in some cases, it has been found necessary to use as many as 10,000 nodes in order to obtain sufficiently accurate results close to the solidus temperature. The simulation then needs approximately 20 iterations, which takes about 20 minutes on an HP* 9000/780/180 with 256 Mb RAM running HP-UX 10.20.

*HP is a trademark of Hewlett-Packard Company, Colorado Springs, CO.

The determination of the pressure and stress are done as a postprocessing operations, using the trapezoidal rule for numerical integration of Eq. [A8] for determining the liquid pressure and simple numerical differentiation of the solid velocity for obtaining the stress, and thereby the pressure, of the solid phase.

REFERENCES

1. J. Campbell: *Castings*, Butterworth Heinemann, London, 1991.
2. M.L. Nedreberg: Ph.D. Thesis, University of Oslo, Oslo, 1991.
3. W.S. Pellini: *Foundry*, 1952, pp. 125-33 and 192-99.
4. B.G. Thomas, I.V. Samarasekera, and J.K. Brimacombe: *Metall. Trans. B*, 1988, vol. 19B, pp. 277-87.
5. B.G. Thomas, I.V. Samarasekera, and J.K. Brimacombe: *Metall. Trans. B*, 1988, vol. 19B, pp. 289-301.
6. J.A. Spittle and A.A. Cushway: *Met. Technol.*, 1983, vol. 10, pp. 6-13.
7. D. Warrington and D.G. McCartney: *Cast Met.*, 1989, vol. 2, pp. 134-43.
8. A.R.E. Singer and S.A. Cottrell: *J. Inst. Met.*, 1947, vol. 73, pp. 33-54.
9. Y.F. Guven and J.D. Hunt: *Cast Met.*, 1988, vol. 1, pp. 104-11.
10. T.W. Clyne and G.J. Davies: *Br. Foundrymen*, 1981, vol. 74, pp. 65-73.
11. U. Feurer: *Gießerei-Forschung*, 1976, vol. 28, pp. 75-80.
12. M. Rappaz, J.-M. Drezet, and M. Gremaud: *Metall. Mater. Trans. A*, 1999, vol. 30A, pp. 449-55.
13. J.-M. Drezet and M. Rappaz: *1st ESAFORM Conf. on Material Forming*, J.L. Chenot, J.F. Agassant, P. Montmitonnet, B. Vergnes, and N. Billon, eds., ESAFORM, Sophia Antipolis, France, 1998, pp. 49-52.
14. J.-M. Drezet and M. Rappaz: in *Modelling of Casting, Welding and Advanced Solidification Processes—VIII*, B.G. Thomas and C. Beckermann, eds., TMS, San Diego, CA, 1998, pp. 883-90.
15. G.K. Sigworth: *AFS Trans.*, 1999, vol. 106, pp. 1053-69.
16. J. Ni and C. Beckermann: *Metall. Trans. B*, 1991, vol. 22B, pp. 349-61.
17. E. Haug and H.J. Thevik: Technical Report STP33 A93019, SINTEF, Norway, 1993.
18. C.Y. Wang and C. Beckermann: *Metall. Mater. Trans. A*, 1996, vol. 27A, pp. 2754-64.
19. G.M. Pharr and M.F. Ashby: *Acta Metall.*, 1983, vol. 31, pp. 129-38.
20. J.-M. Drezet and G. Eggeler: *Scripta Metall.*, 1994, vol. 31, pp. 757-62.
21. P. Vicente-Hernandez, F. Decultieux, P. Schmidt, I.L. Svensson, and C. Levaillant: *Iron Steel Inst. Jpn. Int.*, 1995, vol. 35, pp. 805-12.
22. P. Wisniewski and H.D. Brody: in *Modeling and Control of Casting and Welding Processes V*, M. Rappaz, M.R. Özgü, and K.W. Mahin, eds., TMS-AIME, Warrendale, PA, 1991, pp. 273-78.
23. P. Ackermann and W. Kurz: *Mater. Sci. Eng.*, 1985, vol. 75, pp. 79-86.
24. S.A. Metz and M.C. Flemings: *AFS Trans.*, 1970, vol. 78, pp. 453-60.
25. T.G. Nguyen, D. Favier, and M. Suery: *Int. J. Plasticity, 1994*, vol. 10, pp. 663-93.
26. A.K. Dahle and L. Arnberg: *Acta Mater.*, 1997, vol. 45, pp. 547-99.
27. A.K. Dahle and D.H. StJohn: *Acta Mater.*, 1999, vol. 47, pp. 31-41.
28. H. Iwasaki, T. Mori, M. Mabuchi, and K. Higashi: *Acta Mater.*, 1998, vol. 46, pp. 6351-60.

29. M. Rappaz and P. Thévoz: *Acta Metall.*, 1987, vol. 35, pp. 1487-97.
30. M. Rappaz and P. Thévoz: *Acta Metall.*, 1987, vol. 35, pp. 2929-33.
31. P.C. Carman: *Flow of Gases through Porous Media*, Butterworth Scientific, London, 1956.
32. S. Asai and I. Muchi: *Trans. Iron Steel Inst. Jpn.*, 1978, vol. 18, pp. 90-98.
33. J. Campbell: *Trans. TMS-AIME*, 1969, vol. 245, pp. 2325-34.
34. J. Campbell and T.W. Clyne: *Cast Met.*, 1991, vol. 3, pp. 224-26.
35. H.G. Fjaer and A. Mo: *Metall. Trans. B*, 1990, vol. 21B, pp. 1049-61.
36. C.L. Martin, D. Favier, and M. Suéry: *Int. J. Plasticity*, 1997, vol. 13, pp. 215-35.
37. C.L. Martin, D. Favier, and M. Suéry: *Int. J. Plasticity*, 1997, vol. 13, pp. 37-259.
38. J. Campbell: *Metallography*, 1971, vol. 4, pp. 269-78.
39. T.S. Piwonka and M.C. Flemings: *Trans. TMS-AIME*, 1966, vol. 236, pp. 1157-65.
40. E. Haug, A. Mo, and H. Thevik: *Int. J. Heat Mass Transfer*, 1995, vol. 38, pp. 1553-63.
41. C.A. Fletcher: *Computational Techniques for Fluid Dynamics*, vol. 1, 2nd ed., Springer-Verlag, Berlin, Heidelberg, New York, 1991.